Eur. Phys. J. D **5**, 135–144 (1999)

THE EUROPEAN PHYSICAL JOURNAL D

EDP Sciences

Spatial and angular distributions of third harmonic generation from metal surfaces

D. Carroll and X.H. Zheng[a]

Department of Pure and Applied Physics, The Queen's University of Belfast, Belfast BT7 1NN, Northern Ireland

Received: 20 May 1998 / Received in final form: 25 August 1998 / Accepted: 1st September 1998

Abstract. Third harmonic generation from planar and spherical metal surfaces is studied theoretically through the standard Green function method, so that the results are not affected by the uncertainty associated with previous simplified models. In general the pattern of the non-linear scattering loosely resembles the pattern of Mie scattering. The strong backward scattering is uniquely related to the non-linear process. These results differ significantly from the predictions of the surface charge model.

PACS. 03.80.+r General theory of scattering – 42.65.Ky Harmonic generation, frequency conversion – 61.46.+w Clusters, nanoparticles, and nanocrystalline materials

1 Introduction

Third harmonic generation (THG) from microscopic metal spheres has attracted extensive interest. On the one hand, the size and geometry of these spheres may alter THG and other non-linear processes substantially [1–3]. On the other hand, the pattern of THG scattering provides a rich wealth of information to probe the nature of these altered processes. However, to our knowledge, detailed spatial and angular distributions of THG from metal spheres have not been predicted successfully.

The general approach to treat THG from microscopic metal spheres has long been established. The incident radiation is resolved into partial waves, which are matched to the partial waves internal to the metal sphere, and to the external partial waves representing scattered light in air. Much of the energy of the internal partial waves is restricted to a thin layer beneath the surface of the sphere, due to the electric conductivity of the metal. THG from this layer is integrated together, and matched to partial waves at the third harmonic outside the sphere. The standard method to integrate THG is the Green function method [4].

On account of the demanding nature of the above general approach, there have been numerous attempts to use simplified models to calculate THG and other non-linear processes from microscopic metal spheres. For example, Hache *et al.* [5] studied very small spheres to ignore the effect of retardation. This means that the high frequency radiation is treated as static, so that both the electric and magnetic fields become the gradient of a scalar potential, which is relatively easy to deal with mathematically. Agarwal *et al.* [6] devised the so-called T-matrix approach, an iteration method, where the first approximation to the THG field is the Mie field, which is relatively simple. The rest of the calculation is fairly straightforward. The purpose of [5,6] is to find the macroscopic susceptibility of the ensemble of spherical non-linear grains. Chew *et al.* [7] developed a method which is in fact a less concise form of the standard Green function method. This method was used by Hill *et al.* [8] to study the third order sum frequency (TOSF) generation from dielectric spheres. However, they only found the total TOSF output, which was shown to depend on the overlap between the TOSF and Mie fields. Dewitz *et al.* [9] used the surface charge method of Östling *et al.* [10] to find the angular distributions of non-linear scattering from microscopic metal spheres. The metal is assumed to be highly conductive, so that there is no electric field inside the metal sphere. Consequently, there is no electric field at the surface of the sphere, save that in the radial direction (surface charge), as the source of various non-linear effects. This surface charge, as well as its counterparts at higher harmonics, has only one component, so that they can be represented and expanded by scalar spherical harmonics. One has to start from the second harmonic generation to study THG, which is in turn the starting point to study higher harmonic generations. The derivation is very involved.

We use the standard Green function method to study the spatial and angular distributions of THG from microscopic metal spheres. No additional assumptions are involved so that the physics of the problem will not be affected by the uncertainties associated with simplified models. All but one element of the third order tensor susceptibility are suppressed in properly selected local coordinate systems. While this exact treatment reveals little about THG polarization in the laboratory system, this is of little consequence when the Green function is integrated

[a] e-mail: xhz@qub.ac.uk

numerically. The spatial distribution of THG shows for example the similarities and differences between the Mie field and THG field, as well as the underlying reasons. In general, the THG field loosely resembles the Mie field, but the former has much stronger backward scattering. We compare our results with previous approximations, in particular the surface charge model, and find significant differences.

Although our major interest lies in microscopic spheres, our study starts from planar metal surfaces, for which various novel results are presented. We use the Green function method to find how THG varies against the angle of incidence, which has not been given previously. By ignoring the effect of dispersion, we find a new analytic formula for the angular variation of THG, which is fairly accurate. We compare this analytic formula with the formula (also new and analytic) derived from the surface charge model, and find significant differences. The simplicity of these formulae, due to the simple geometry of the planar metal surface, leaves little doubt that the surface charge model is not a valid alternative to the Green function method. Bloembergen *et al.* [12] studied the second harmonic generation (SHG) from the planar surface of a non-linear material. However, they did not use the Green function method. Furthermore, they were interested in critical phenomena, such as the equivalent Brewster angle and total reflection for harmonic waves, rather than the angular variation of THG.

Throughout our discussion, we assume the metal surface is in air, whose refractive index is $n_1 = 1.00$ at all harmonics. We will use iron as an example, whose refractive index is $n_2 = 2.88 + 3.05i$ at $\lambda = 617$ nm but $n_2^{(3)} = 1.49 + 1.41i$ at the third harmonic [11]. The diameter of the iron sphere varies between 0 and 20 μm. In Section 2 we introduce the Green function *via* a study of THG from a planar metal surface. We ignore dispersion, so that $n_2 = n_2^{(3)}$. In Section 3 we consider the effect of dispersion. In Section 4 we use the surface charge model to study THG from planar metal surfaces. We study microscopic metal spheres in Section 5. The THG scattering is found from the standard Green function method, and the numerical results are listed in Section 6, to be compared with the surface charge model for metal spheres in Section 7. Brief conclusions are given in Section 8.

2 Planar metal surface without dispersion

We use the Green function method to study THG from a planar metal surface (Fig. 1). For simplicity we ignore the effect of dispersion. We discuss this problem in some detail to appreciate the nature of the method. This will help us in later discussions, which may be obscured by the rather lengthy mathematics in spherical co-ordinates. The incident light makes an angle θ_i to the normal of the metal surface, so that the wave vector of this incident light is

$$\mathbf{k}_1 = kn_1(\hat{\mathbf{x}}\sin\theta_i + \hat{\mathbf{z}}\cos\theta_i) \tag{2.1}$$

where $k = \omega/c$ is the wave number in vacuum, ω and c the angular frequency and speed of the light in vacuum,

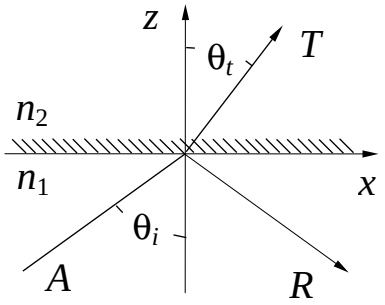

Fig. 1. Ray paths at the planar surface of a metal covered by a medium. The incident, reflected and transmitted rays are marked by A, R and T respectively, θ_i and θ_t are angles of incidence and transmission. The refractive index is n_1 in the medium but n_2 in the metal.

$\hat{\mathbf{x}}$, $\hat{\mathbf{y}}$ and $\hat{\mathbf{z}}$ unit vectors in the x, y and z-directions, respectively. Similarly, the wave vector of the transmitted light is

$$\mathbf{k}_2 = kn_2(\hat{\mathbf{x}}\sin\theta_t + \hat{\mathbf{z}}\cos\theta_t) \tag{2.2}$$

where θ_t is the angle of transmission. The amplitude $T_\perp$ of the transmitted light is found from the Fresnel formula [13]

$$T_\perp = \frac{2n_1\cos\theta_i}{n_1\cos\theta_i + n_2\cos\theta_t}A_\perp. \tag{2.3}$$

Here $A_\perp$ is the amplitude of the incident light, the subsymbol $\perp$ indicates TE polarization, that is, the electric field of the light is in the y-direction, perpendicular to the plane of incidence (x–z plane). Since the incident and transmitted light must be in phase at the surface of the metal, we have $(\mathbf{k}_1 - \mathbf{k}_2)\cdot\hat{\mathbf{x}} = 0$ at $z = 0$, leading through equations (2.1, 2.2) to Snell's law [13]

$$n_2\sin\theta_t = n_1\sin\theta_i \tag{2.4}$$

which is real, despite n_2 being complex. On the other hand,

$$n_2\cos\theta_t = \sqrt{n_2^2 - n_2^2\sin^2\theta_t} = \sqrt{n_2^2 - n_1^2\sin^2\theta_i} \tag{2.5}$$

is complex, the imaginary part indicating how quickly light attenuates towards the interior of the metal (in the z-direction, see Fig. 1). Equations (2.1–2.5) enable us to evaluate the electric field of the transmitted light

$$\mathbf{E}_\perp(\mathbf{r}, t) = \hat{\mathbf{y}}T_\perp\exp[i(\mathbf{k}_2\cdot\mathbf{r} - \omega t)] \tag{2.6}$$

where $\mathbf{r} = \hat{\mathbf{x}}x + \hat{\mathbf{z}}z$.

Now we consider THG light at 3ω. Since we have ignored dispersion, equations (2.1, 2.2) still apply. The electric field of the THG light is given by

$$\mathbf{E}^{(3)}(\mathbf{r}, t) + c.c. = \int G(\mathbf{r}, \mathbf{r}')\mathbf{J}(\mathbf{r}', t)d\mathbf{r}' \tag{2.7}$$

where the Green function

$$G(\mathbf{r}, \mathbf{r}') = \frac{\exp[i3kn_2(z - z')\cos\theta_t]}{i6kn_2\cos\theta_t} \tag{2.8}$$

which applies when $z > z'$, otherwise z and z' must be interchanged in equation (2.8). It is clear that equation (2.7) integrates THG from a layer beneath the metal surface. The non-linear displacement current density $\mathbf{D} = \varepsilon\Sigma\mathbf{E} + \chi^{(3)}(\Sigma\mathbf{E})^3$ leads through the wave equation $\nabla^2\Sigma\mathbf{E} = \mu\partial^2\mathbf{D}/\partial t^2$ to a non-linear term $\mathbf{J} = \mu\chi^{(3)}\partial^2(\Sigma\mathbf{E})^3/\partial t^2$ which can be seen as the THG current density, where μ is the permeability, $\chi^{(3)}$ the third order tensor susceptibility of the metal, and $\Sigma\mathbf{E}$ the electric field involving all harmonics. As a good approximation, we replace $\Sigma\mathbf{E}$ with $\mathbf{E}_\perp + c.c.$ so that

$$\mathbf{J} = -\hat{\mathbf{y}}(3k)^2 T_\perp^{(3)} \exp[i3(\mathbf{k}_2 \cdot \mathbf{r} - \omega t)] + c.c. \tag{2.9}$$

where

$$T_\perp^{(3)} = \varepsilon_0^{-1}\chi_{1111}^{(3)} T_\perp^3 \tag{2.10}$$

represents the amplitude of the THG field, ε_0 is the vacuum permittivity, $\chi_{1111}^{(3)}$ an element of $\chi^{(3)}$ [14]. Apparently $T_\perp^{(3)}$ has the dimensions of an electric field. We have dropped from equation (2.9) terms not proportional to $\exp(\pm i3\omega t)$, because they do not contribute to THG. Note that the integration in equation (2.7) is reduced to 1D, giving

$$\mathbf{E}_\perp^{(3)} = T_\perp^{(3)} \left[\hat{\mathbf{y}} \frac{-1 + i6kn_2 z\cos\theta_t}{(2n_2\cos\theta_t)^2}\right] \exp[i3(\mathbf{k}_2 \cdot \mathbf{r} - \omega t)] \tag{2.11}$$

which leads through Maxwell's equations to

$$\mathbf{H}_\perp^{(3)} = n_2\sqrt{\frac{\varepsilon_0}{\mu_0}} T_\perp^{(3)} \left[\hat{\mathbf{x}} \frac{-1 - i6kn_2\cos\theta_t}{(2n_2\cos\theta_t)^2}\cos\theta_t + \hat{\mathbf{z}} \frac{-1 + i6kn_2 z\cos\theta_t}{(2n_2\cos\theta_t)^2}\sin\theta_t\right] \exp[i3(\mathbf{k}_2 \cdot \mathbf{r} - \omega t)] \tag{2.12}$$

as the magnetic field density of the THG light.

In order to test whether THG is observable in the medium outside the metal, we use equations (2.11, 2.12) to calculate the Poynting vector. When $z = 0$, we find

$$\mathbf{S} = \mathrm{Re}(\mathbf{E} \times \mathbf{H}^*) = \sqrt{\frac{\varepsilon_0}{\mu_0}} |T_\perp^{(3)}|^2 \frac{\mathrm{Re}(\hat{\mathbf{x}} n_2 \sin\theta_t - \hat{\mathbf{z}} n_2 \cos\theta_t)}{|2n_2\cos\theta_t|^4} \tag{2.13}$$

where * indicates complex conjugation. This is directed toward the outside of the metal. Some of the outgoing THG light is transmitted into the medium, the rest is reflected back into the metal. By matching the electric and magnetic fields of the transmitted and reflected THG light with $\mathbf{E}^{(3\omega)}$ and $\mathbf{H}^{(3\omega)}$ in equations (2.11, 2.12), we find

$$\frac{-T_\perp^{(3)}}{2n_2\cos\theta_t(n_1\cos\theta_i + n_2\cos\theta_t)} \tag{2.14}$$

as the amplitude of the observed THG light, which leaves the metal along R in Figure 1. The energy flux of the observed THG light is found from equations (2.3, 2.10, 2.14) to be

$$n_1\sqrt{\frac{\varepsilon_0}{\mu_0}} |\varepsilon_0^{-1}\chi_{1111}^{(3)} A_\perp^3|^2 \frac{16}{|n_2\cos\theta_t|^2} \frac{|n_1\cos\theta_i|^6}{|n_1\cos\theta_i + n_2\cos\theta_t|^8} \tag{2.15}$$

which is plotted in Figure 2a.

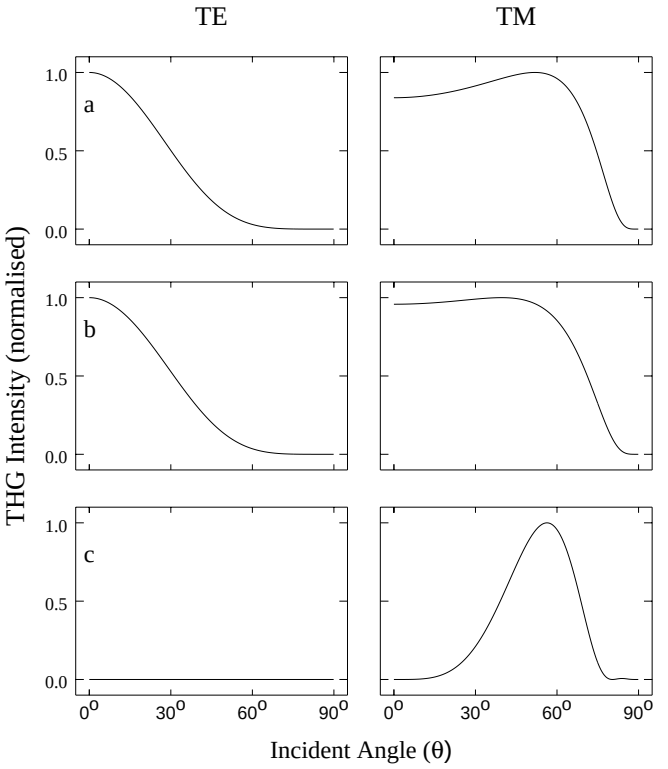

Fig. 2. Normalized intensities of THG scattering from a planar metal surface. The polarization is TE and TM in the left and right columns, respectively. Dispersion is neglected in row (a) but considered in row (b). The surface charge model in row (c) gives no THG for TE polarization.

The derivation is similar when the polarization is TM (the magnetic field of the incident light is in the y-direction, see Fig. 1). Equation (2.3) is replaced by

$$T_\parallel = \frac{2n_1\cos\theta_i}{n_2\cos\theta_i + n_1\cos\theta_t} A_\parallel \tag{2.16}$$

where the sub-symbol $\parallel$ indicates TM polarization. Equation (2.10) is replaced by

$$T_\parallel^{(3)} = \varepsilon_0^{-1}\chi_{1111}^{(3)} T_\parallel^3. \tag{2.17}$$

The amplitude of the observed THG light becomes

$$\frac{-T_\parallel^{(3)}\cos 2\theta_t}{2n_2\cos\theta_t(n_2\cos\theta_i + n_1\cos\theta_t)} \tag{2.18}$$

whereas the energy flux of the THG light becomes

$$n_1\sqrt{\frac{\varepsilon_0}{\mu_0}}|\varepsilon_0^{-1}\chi^{(3)}_{1111}A_\parallel^3|^2\frac{16|\cos 2\theta_t|^2}{|n_2\cos\theta_t|^2}\frac{|n_1\cos\theta_i|^6}{|n_2\cos\theta_i+n_1\cos\theta_t|^8} \tag{2.19}$$

which is also plotted in Figure 2a.

3 Planar metal surface with dispersion

In general, the permittivity of a metal depends on the frequency of light [11]. This was considered by Bloembergen *et al.* [12] in their study of SHG from the planar surface of a non-linear medium. They did not use the Green function but solved the wave equation directly, which is possible for the simple case of Figure 1. When applied to THG, their results are identical to those from the Green function method. We outline these results here, which enable us to find the angular variation of THG from planar metal surfaces (to our knowledge not given previously). At the third harmonic, equation (2.2) is replaced by

$$3\mathbf{k}_2^{(3)} = 3kn_2^{(3)}(\hat{\mathbf{x}}\sin\theta_t^{(3)} + \hat{\mathbf{z}}\cos\theta_t^{(3)}) \tag{3.1}$$

where $n_2^{(3)}$ is the refractive index of the metal at the third harmonic, $\theta_t^{(3)}$ the transmission angle of THG light. Equation (2.4) is replaced by

$$n_2^{(3)}\sin\theta_t^{(3)} = n_1\sin\theta_i \tag{3.2}$$

whereas equation (2.5) is replaced by

$$n_2^{(3)}\cos\theta_t^{(3)} = \sqrt{(n_2^{(3)})^2 - n_1^2\sin^2\theta_i}. \tag{3.3}$$

If the polarization is TE, then the electric field density of the THG light becomes

$$\mathbf{E}_\perp^{(3)} = \frac{T_\perp^{(3)}}{n_2^2-(n_2^{(3)})^2}\Big[\hat{\mathbf{y}}\exp(i3\mathbf{k}_2\cdot\mathbf{r}) - \hat{\mathbf{y}}\frac{n_1\cos\theta_i+n_2\cos\theta_t}{n_1\cos\theta_i+n_2^{(3)}\cos\theta_t^{(3)}}\exp(i3\mathbf{k}_2^{(3)}\cdot\mathbf{r})\Big]\exp(-i3\omega t). \tag{3.4}$$

The first term in the square bracket represents a plane wave in phase with the transmitted light T in Figure 1, which is the source of THG. The second term represents THG light propagating on its own. The amplitude of the observed THG light is

$$\frac{-T_\perp^{(3)}}{(n_2\cos\theta_t+n_2^{(3)}\cos\theta_t^{(3)})(n_1\cos\theta_i+n_2^{(3)}\cos\theta_t^{(3)})} \tag{3.5}$$

which can be compared with equation (2.14). If the polarization is TM, then equation (3.4) is replaced by

$$\mathbf{E}_\parallel^{(3)} = \frac{T_\parallel^{(3)}}{n_2^2-n_2^{(3)2}}\Big[(-\hat{\mathbf{x}}\cos\theta_t+\hat{\mathbf{z}}\sin\theta_t)\exp(i3\mathbf{k}_2\cdot\mathbf{r}) - (-\hat{\mathbf{x}}\cos\theta_t^{(3)}+\hat{\mathbf{z}}\sin\theta_t^{(3)})\frac{n_2\cos\theta_i+n_1\cos\theta_t}{n_2^{(3)}\cos\theta_i+n_1\cos\theta_t^{(3)}} \times\exp(i3\mathbf{k}_2^{(3)}\cdot\mathbf{r})\Big]\exp(-i3\omega t) \tag{3.6}$$

whereas equation (3.5) becomes

$$\frac{-T_\parallel^{(3)}[(n_2^{-2}+n_2^{(3)-2})n_1^2\sin^2\theta_i-1]}{(n_2\cos\theta_t^{(3)}+n_3^{(3)}\cos\theta_t)(n_1\cos\theta_t^{(3)}+n_2^{(3)}\cos\theta_i)} \tag{3.7}$$

which is the amplitude of THG light of TM polarization. Values of equations (3.5, 3.7) are plotted in Figure 2b, which are very similar to the approximate THG curves in Figure 2a.

4 Surface charge model for planar metal surface

By definition, the surface charge is the normal component of the electric field of light on the surface of a metal (unit: V/m) [10]. All the tangential components of the field are assumed to vanish. This surface charge model works when the physical process of interest is outside the metal. For example, in a microwave resonator most electromagnetic energy is in the empty cavity. The electric field near the metal wall is so weak that, apart from the field component normal to the wall, it can be safely assumed to be zero. However, the situation is reversed in THG, which takes place inside the metal. This leads to a difficulty: when the polarization of the incident light is TE, there is no surface charge and hence no THG, contrary to equations (3.4, 3.5). When the polarization of the incident light is TM, the THG contribution due to the surface charge is comparable to that from the tangential components of the electric field, and there is no *a priori* justification for ignoring the latter. To show this, we compare expression (3.7) with the prediction of the surface charge model. We add the electric fields of the incident light A and reflected light R together, and subtract from the result the electric field of the transmitted light T (Fig. 1). This cancels all the tangential electric field components of $A+R$ at $z=0$, and the surface charge is found to be

$$\sigma = \left[A_\parallel + R_\parallel - \frac{n_1}{n_2}T_\parallel\right]\sin\theta_i\exp[i(kn_1x\sin\theta_i-\omega t)] \tag{4.1}$$

where $T_\parallel$ is given by equation (2.16), and the Fresnel formula [13] gives

$$R_\parallel = \frac{n_2\cos\theta_i - n_1\cos\theta_t}{n_2\cos\theta_i+n_1\cos\theta_t}A_\parallel \tag{4.2}$$

as the amplitude of reflected light. The surface charge at the third harmonic is assumed to be

$$\sigma^{(3)} = (\sigma + c.c.)^3 \sim \sigma^3 + c.c. \tag{4.3}$$

We have omitted from equation (4.3) all the terms not proportional to $\exp(\pm i3\omega t)$, because they do not contribute to THG. Equation (4.3) is the normal component of THG light on the air-metal interface. This THG light is made from two plane waves coming from and reflected back into the metal, and a third plane wave transmitted into air. The amplitudes of these three waves are dictated by equation (4.3) and the fundamental law that the tangential electric fields of the THG light be continuous across the air-metal boundary [12]. However, another fundamental law, that the tangential magnetic fields of THG light be continuous, cannot be satisfied, due to the introduction of equation (4.3). The amplitude of the THG electric wave in air is

$$\frac{n_1^{-1}\sin^2\theta_i\cos\theta_t}{n_2\cos\theta_i + n_1\cos\theta_t}\left[A_\parallel + R_\parallel - \frac{n_1}{n_2}T_\parallel\right]^3 \tag{4.4}$$

where for simplicity we have ignored the effect of dispersion. Since $\chi^{(3)}$ is not involved in expression (4.4), the strength of THG cannot be predicted in a natural manner. We find the normalized THG energy flux in air from equations (2.16, 4.2, 4.4) as

$$\frac{\sin^4\theta_i\cos^6\theta_i\cos^2\theta_t}{(n_2\cos\theta_i + n_1\cos\theta_t)^8} \tag{4.5}$$

which is plotted in Figure 2c. Equation (4.5) is new, and is significantly different from equation (2.19). This, together with the absence of THG for TE polarization, demonstrates that the surface charge model of THG is fundamentally inadequate, even in the simple case of planar metal surface. Therefore it is not proper to use this model in the case of spherical metal surface [9], as is shown next.

5 Spherical metal surface

We consider a metal sphere illuminated by an incident plane wave, linearly polarized in the x-direction (Fig. 3). We use the Green function in free space [4]

$$\begin{aligned} G(\mathbf{r},\mathbf{r}') = \frac{3k_2^{(3)}}{4\pi i}\sum_{\ell=0}^{\infty}\frac{2\ell+1}{\ell(\ell+1)}\sum_{m,\sigma}\varepsilon_m\frac{(\ell-m)!}{(\ell+m)!} \\ \times[\ell(\ell+1)\mathbf{L}^3_{\sigma m\ell}(\mathbf{r})\mathbf{L}^1_{\sigma m\ell}(\mathbf{r}') \\ + \mathbf{M}^3_{\sigma m\ell}(\mathbf{r})\mathbf{M}^1_{\sigma m\ell}(\mathbf{r}') + \mathbf{N}^3_{\sigma m\ell}(\mathbf{r})\mathbf{N}^1_{\sigma m\ell}(\mathbf{r}')]. \end{aligned} \tag{5.1}$$

Here $3k_2^{(3)} = 3kn_2^{(3)}$ is the wave number in the metal at 3ω, $0 \le m \le \ell$, ε_m is the Neumann factor which has the value 2 when $m = 0$ and 1 when $m > 0$, σ stands for e (even) or o (odd), $\mathbf{r}$ represents the spherical coordinates

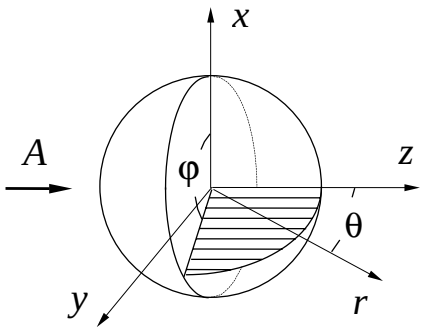

Fig. 3. Scattering by a metal sphere. The incident light, marked by A, is a monochromatic plane wave, linearly polarized in the x-direction. The sphere has radius ρ and is at the centre of the coordinate systems.

r, θ and φ ($\mathbf{r}'$ represents r', θ' and φ'). Furthermore,

$$\begin{aligned} \mathbf{L}^1_{\sigma m\ell} &= \frac{1}{3k_2^{(3)}}\nabla\psi^1_{\sigma m\ell}(\mathbf{r}) \\ \mathbf{M}^1_{\sigma m\ell} &= \nabla\times[\hat{\mathbf{r}}r\psi^1_{\sigma m\ell}(\mathbf{r})] \\ \mathbf{N}^1_{\sigma m\ell} &= \frac{1}{3k_2^{(3)}}\nabla\times\nabla\times[\hat{\mathbf{r}}r\psi^1_{\sigma m\ell}(\mathbf{r})] \end{aligned} \tag{5.2}$$

are solutions of the vector wave equation, $\hat{\mathbf{r}}$ being the radial unit vector,

$$\psi^1_{em\ell}(\mathbf{r}) = j_\ell(3k_2^{(3)}r)P^m_\ell(\cos\theta)\cos m\varphi \tag{5.3}$$

with P^m_ℓ being the associated Legendre function, σ having taken the value e for even symmetry. If $\sigma = o$ then $\cos m\varphi$ in equation (5.3) should be replaced by $\sin m\varphi$. When the upper index of ψ is not 1 but 3, j_ℓ should be replaced by $h^{(1)}_\ell$ (both are spherical Bessel functions) [12,15]. So far we have assumed $r > r'$, otherwise the upper indices of $\mathbf{L}$, $\mathbf{M}$ and $\mathbf{N}$ in equation (5.1) must be interchanged. The Green function in equation (5.1) is a dyadic, which represents a vector point source, similar to the familiar scalar point source $\exp(ik|\mathbf{r}-\mathbf{r}'|)/k|\mathbf{r}-\mathbf{r}'|$ in a vacuum.

In the metal sphere the THG current density is given by (see Sect. 2)

$$\begin{aligned} \mathbf{J}(\mathbf{r},t) &= \mu\chi^{(3)}_{1111}\frac{\partial^2}{\partial t^2}[\mathbf{E}_{mie}(\mathbf{r},t) + c.c.]^3 \\ &\sim -(3k)^2T^{(3)}(|\mathbf{u}|^2 - |\mathbf{v}|^2 + 2i\mathbf{u}\cdot\mathbf{v})(\mathbf{u}+i\mathbf{v}) \\ &\quad\times\exp(-i3\omega t) + c.c. \end{aligned} \tag{5.4}$$

where $\mathbf{E}_{mie}(\mathbf{r},t) = A_{mie}(\mathbf{u}+i\mathbf{v})\exp(-i\omega t)$ is the electric field inside the metal sphere, A_{mie} being the amplitude of the incident plane wave,

$$T^{(3)} = \varepsilon_0^{-1}\chi^{(3)}_{1111}A^3_{mie} \tag{5.5}$$

which has the dimensions of electric field density. The first line of equation (5.4) means that $\mathbf{J}$ is parallel to $\mathbf{E}_{mie} + c.c.$ whereas $|\mathbf{J}|$ is proportional to $|\mathbf{E}_{mie} + c.c.|^3$. To see this, consider a local Cartesian coordinate system

where $\mathbf{E}_{mie} + c.c.$ is parallel to the x-axis. Then in THG the electric fields of all three incident waves are in the x-direction, which suppresses 20 of the 21 non-zero tensor elements, leaving $\mathbf{J}$ in the x-direction [14]. On the other hand, had $\mathbf{J}$ had a component in say the y-direction, the tensor element $\chi^{(3)}_{2111}$ would have been non-zero [14]. The second line of equation (5.4) is found by expanding the first line and keeping terms proportional to $\exp(\pm i3\omega t)$, because other terms do not contribute to THG. According to Mie theory [13,16]

$$\mathbf{u} + i\mathbf{v} = \sum_{\ell=1}^{\infty} i^{\ell+1} \frac{2\ell+1}{\ell(\ell+1)} [a_\ell^{TE} \mathbf{M}^1_{o1\ell}(\mathbf{r}) + a_\ell^{TM} \mathbf{N}^1_{e1\ell}(\mathbf{r})] \tag{5.6}$$

where $\mathbf{M}$ and $\mathbf{N}$ are defined by equations (5.2, 5.3), $3k_2^{(3)}$ being replaced by $k_2 = |\mathbf{k}_2|$, because equation (5.6) applies not at 3ω but at ω, where $\mathbf{k}_2$ is given by equation (2.2). We also have

$$a_\ell^{TE} = \frac{n_2}{\psi_\ell(n_2 k\rho)\zeta_\ell^{(1)'}(k\rho) - n_2\psi'_\ell(n_2 k\rho)\zeta_\ell^{(1)}(k\rho)} \tag{5.7}$$

$$a_\ell^{TM} = \frac{-in_2}{n_2\psi_\ell(n_2 k\rho)\zeta_\ell^{(1)'}(k\rho) - \psi'_\ell(n_2 k\rho)\zeta_\ell^{(1)}(k\rho)} \tag{5.8}$$

where ρ is the radius of the metal sphere, ψ_ℓ and $\zeta_\ell^{(1)}$ are Ricatti-Bessel functions [15], a prime over these functions denoting differentiation with respect to the argument.

In equation (5.4) $|\mathbf{r}| \le \rho$ must hold, because there is no THG current outside metal sphere. To simplify our argument, we consider THG radiation just beneath the surface of the sphere, so that $|\mathbf{r}| = \rho$. This means that, when we substitute equations (5.1, 5.4) into equation (2.7), $r \ge r'$ always holds, and there is no need to change the upper indices of $\mathbf{M}$ and $\mathbf{N}$ in equation (5.1). We will drop $\mathbf{L}$ from equation (5.1), otherwise $\nabla \cdot \mathbf{E}^{(3)}$ will not vanish, inconsistent with the fact that in THG the effect of free charges is negligible [13]. We are free to do so, because $\mathbf{E}^{(3)}$ incorporates a scalar potential not yet specified. The electric field of the THG light is found to be

$$\mathbf{E}^{(3)}(\mathbf{r},t) = T^{(3)} \sum_{\ell=0}^{\infty} \frac{2\ell+1}{\ell(\ell+1)} \sum_{\sigma,m} \frac{(\ell-m)!}{(\ell+m)!} \times [b_{\sigma ml}^{TE} \mathbf{M}^3_{\sigma m\ell}(\mathbf{r}) + b_{\sigma ml}^{TM} \mathbf{N}^3_{\sigma ml}(\mathbf{r})] \exp(-i3\omega t) \tag{5.9}$$

where $|\mathbf{r}| = \rho, T^{(3)}$ is defined by equation (5.5),

$$b_{\sigma m\ell}^{TE} = \frac{-(3k)^3 n_2}{4\pi i} \int \mathbf{M}^1_{\sigma m\ell}(\mathbf{r})(|\mathbf{u}|^2 - |\mathbf{v}|^2 + 2i\mathbf{u}\cdot\mathbf{v})(\mathbf{u} + i\mathbf{v}) d\mathbf{r} \tag{5.10}$$

$$b_{\sigma m\ell}^{TM} = \frac{-(3k)^3 n_2}{4\pi i} \int \mathbf{N}^1_{\sigma m\ell}(\mathbf{r})(|\mathbf{u}|^2 - |\mathbf{v}|^2 + 2i\mathbf{u}\cdot\mathbf{v})(\mathbf{u} + i\mathbf{v}) d\mathbf{r} \tag{5.11}$$

$\mathbf{M}$ and $\mathbf{N}$ being given by equations (5.2, 5.3), whereas $\mathbf{u}$ and $\mathbf{v}$ being given by equation (5.6).

Equation (5.9) applies only at $|\mathbf{r}| = \rho$, because when $|\mathbf{r}| > \rho$ the refractive index changes. On the other hand, equation (5.1) is the Green function in free space, where the refractive index is constant. The THG radiation outside the metal sphere is found from the following physical consideration [8]. At the boundary of the metal sphere, some energy of $\mathbf{E}^{(3)}$ in equation (5.9) is reflected back into the sphere to generate an internal field, which is a series in $\mathbf{M}^1_{\sigma m\ell}(\mathbf{r})$ and $\mathbf{N}^1_{\sigma m\ell}(\mathbf{r})$, similar to equation (5.6) but at the third harmonic. This internal field and $\mathbf{E}^{(3)}$ are added together to give the electric field of THG light on the metal surface. The magnetic field of the THG light is then found from Maxwell's equation. The tangential components of these THG fields are continuous across the metal-air boundary, and this defines THG radiation in air. As a result, we find the electric field of the THG radiation in air as

$$T^{(3)} \sum_{\ell=0}^{\infty} \frac{2\ell+1}{\ell(\ell+1)} \sum_{\sigma,m} \frac{(\ell-m)!}{(\ell+m)!} \times [c_{\sigma m\ell}^{TE} \mathbf{M}^3_{\sigma m\ell}(\mathbf{r}) + c_{\sigma m\ell}^{TM} \mathbf{N}^3_{\sigma m\ell}(\mathbf{r})] \exp(-i3\omega t). \tag{5.12}$$

$\mathbf{M}$ and $\mathbf{N}$ are given by equations (5.2, 5.3), with $3k_2^{(3)}$ being replaced by $3k$, the wave number at 3ω in air. Furthermore

$$c_{\sigma m\ell}^{TE} = \frac{b_{\sigma m\ell}^{TM}}{\psi_\ell(3n_2^{(3)}k\rho)\zeta_\ell^{(1)'}(3k\rho) - n_2^{(3)}\psi'_\ell(3n_2^{(3)}k\rho)\zeta_\ell^{(1)}(3k\rho)} \tag{5.13}$$

$$c_{\sigma m\ell}^{TM} = \frac{i\, b_{\sigma m\ell}^{TM}}{n_2^{(3)}\psi_\ell(3n_2^{(3)}k\rho)\zeta_\ell^{(1)'}(3k\rho) - \psi'_\ell(3n_2^{(3)}k\rho)\zeta_\ell^{(1)}(3k\rho)} \tag{5.14}$$

where $b_{\sigma m\ell}^{TE}$ and $b_{\sigma m\ell}^{TM}$ are given by equations (5.10, 5.11). Equations (5.13, 5.14) can be compared with their counterparts equations (2.14, 2.18, 3.5, 3.7) for THG scattering by the planar metal surface. The magnetic field of scattered THG light can be readily found from equation (5.12) through Mie theory. The density of energy flux of THG scattering is found from the first line of equation (2.13).

6 Numerical results

The integrations in equations (5.10, 5.11) are three dimensional (3D), which represents a large amount of computation. However, the Mie field in equation (5.6) has a simple dependence on φ, so that the integration in φ can be performed analytically, that is equations (5.10, 5.11) are actually 2D with respect to numerical integration. Furthermore the analytical integration in φ leads to a selection rule that, unless $m = 1$ or 3, $c_{\sigma m\ell}^{TE}$ and $c_{\sigma m\ell}^{TM}$ in equations (5.10, 5.11) will vanish, significantly reducing the number of terms in equations (5.9, 5.12) (there is a different selection rule in [8], because the standard Green function is not used there).

We evaluate equations (5.6, 5.9, 5.12), truncate the series when the desired accuracy is attained, which in our

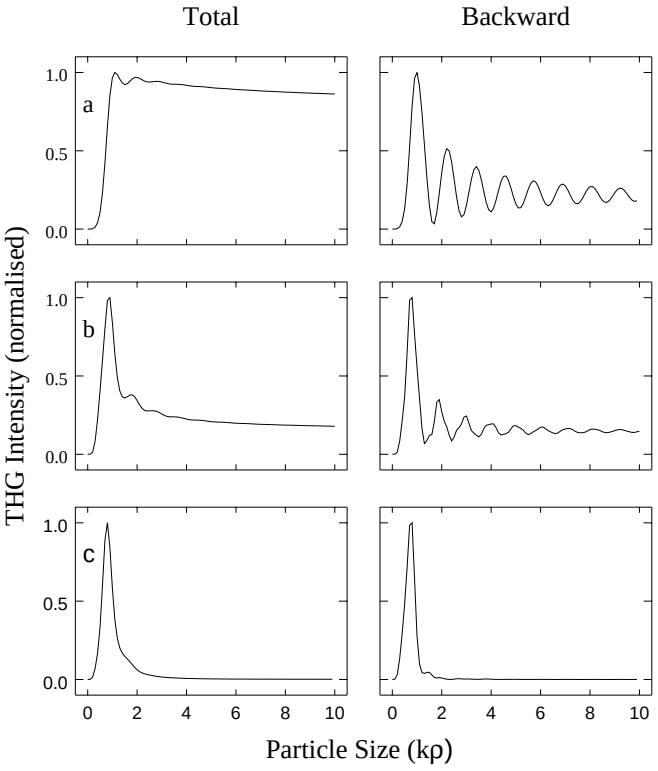

Fig. 4. Normalized cross-sections of total (left column) and backward (right column) scattering: row (a) Mie scattering, row (b) THG scattering and row (c) THG scattering from the surface charge model.

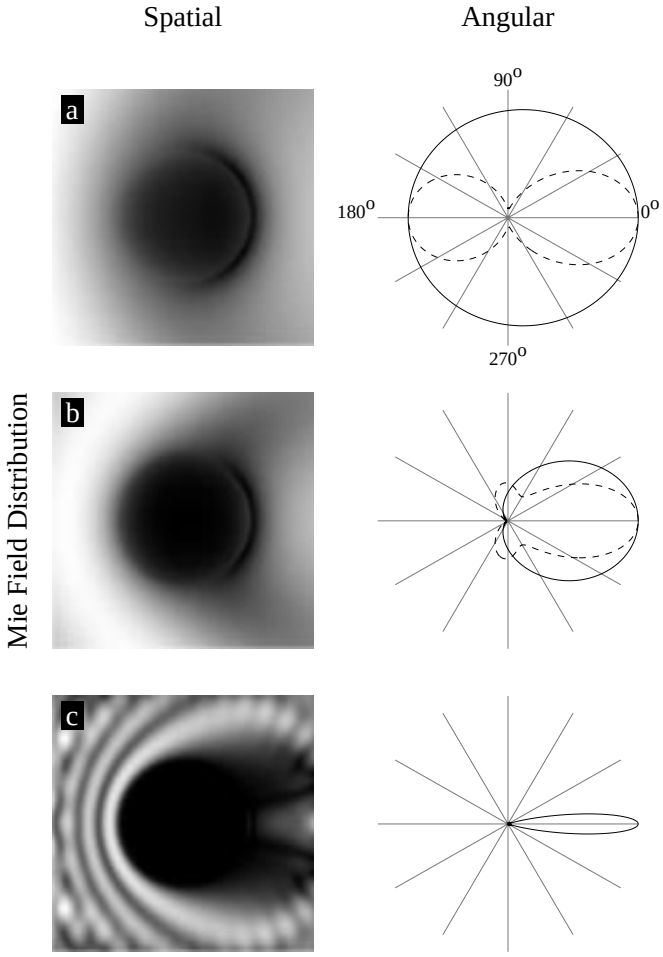

Fig. 5. Spatial (left column) and angular (right column) distributions of the electric Mie field in the $\varphi = 90^\circ$ plane. The linear grey scale is proportional to the absolute value of the field (lighter gray for higher values). The broken and solid lines in the polar plots represent the intensities of the field components seen through a polarizer at $\varphi = 0^\circ$ and 90°, respectively. Row (a) $k\rho = 0.975\,45$, row (b) $k\rho = 1.663\,37$ and row (c) $k\rho = 10.000\,00$ (broken line dropped for clarity).

case is $\ell \approx 50$ for THG at $x = 10$. We use the Newton-Cotes formula of the 10th order for numerical integration [15]. The number of divisions of the integration interval is chosen to be 5 times the number of zeros of $\mathbf{M}$ or $\mathbf{N}$ in equation (5.1). For example, the Legendre function $P_\ell^m(\cos\theta)$ has ℓ zeros for $0 \le \theta \le \pi$, so that the number of divisions is 5ℓ. To check the accuracy of the above integration scheme, we study coherent fluorescence from a dielectric micro-sphere. We replace equation (5.4) with the Mie field $\mathbf{J} = \alpha(\mathbf{u}+i\mathbf{v})\exp(-i\omega t)$, α being a constant and $\mathbf{u}+i\mathbf{v}$ given in equation (5.6). As a result, we are able to evaluate equation (2.7) both analytically and numerically. The analytical result is virtually identical to that in [7]. The relative error in the numerical result is at worst $\sim 5\%$ in directions of θ where fluorescence is extremely weak. In most directions the error is much smaller.

We define the (normalized) total cross-section of scattering as $W_{total}/\pi\rho^2$, W_{total} being the scattered energy into a 4π solid angle and ρ the radius of the sphere. We also define the (normalized) cross-section of backward scattering as $W_{back}/\pi\rho^2$, W_{back} being the scattered energy into unit solid angle about $\theta = 180^\circ$.

We compare Mie scattering and THG scattering. In Figure 4a the total cross-section of Mie scattering increases quickly until $k\rho \approx 1$, and becomes fairly flat thereafter. In Figure 4b the total cross-scattering of THG scattering also increases until $k\rho \approx 1$, but drops sharply at larger $k\rho$. It appears that when the metal sphere is small the incident light may penetrate the whole interior of the sphere, giving more THG for larger spheres, until $k\rho \approx 1$. When the sphere becomes larger still, the metal ball start to block the incident light, so that THG drops. On the other hand, Mie scattering and THG scattering appear to share more common features in the backward direction. For example, both have a strong peak at $k\rho \approx 1$ and oscillate thereafter, although the oscillation of THG scattering is more heavily damped.

In Figure 5 we plot spatial and angular distributions of Mie scattering at $k\rho = 0.975\,45$, $1.663\,37$ and $10.000\,00$, for which the back scattering reaches its first maximum, its first minimum, and a representative relatively large value of $k\rho$, respectively. It is clear from the spatial and angular distributions that the metal sphere casts almost

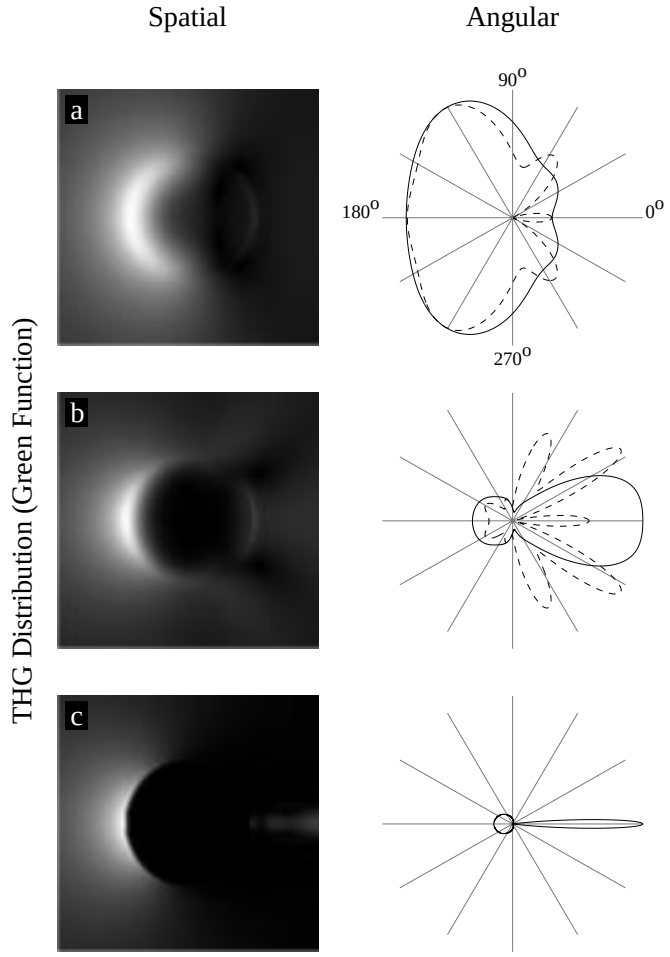

Fig. 6. Spatial and angular distributions of the electric field of THG scattering. The conventions are the same as those in Figure 5.

no shadow. The incident light is blocked only in a narrow region immediately behind the sphere ($r \approx \rho, |\theta| < 90°$), reminiscent of the well-known fact that, when a few Fresnel zones are blocked, the incident light may be focused into the shadow. Indeed, there is always a peak around $\theta = 0°$ in the angular distributions of Mie scattering.

In Figure 6 we plot spatial and angular distributions of THG light for the same $k\rho$ values. In general, there is loose resemblance between the THG and Mie distributions, particularly when $k\rho$ is large. The reason for this appears to lie in the Huygens principle, according to which the wave front of the Mie scattering is the envelop of spherical wavelets emitted by a previous wave front. In THG this previous wave front also emits wavelets at the third harmonic to produce the THG scattering, which must bear some resemblance to the Mie scattering, such as having a peak around $\theta = 0°$. On the other hand, while the THG distributions always have a sizeable lobe around $\theta = 180°$, the Mie distributions have not. The reason for this difference may be appreciated from Figure 5, where the incident light is always blocked in a narrow shadow area immediately behind the metal sphere. Therefore THG is strong when the sphere is illuminated directly by the incident light, as is clear from Figure 6, which leads to the strong backward THG scattering.

7 Surface charge model for spherical metal surface

We outline the surface charge approach to the study of THG by metal spheres. We study both the spatial and angular distributions of THG light. The former was not studied previously, but is important for us to understand the inadequacy of this model. We incorporate numerical methods into our study wherever convenient. The "full" analytic solutions of Dewitz *et al.* [9] and Östling *et al.* [10] are very involved and, in the end of the day, also have to be evaluated numerically. The surface charge is found to be

$$\sigma = (n_2^2 - 1)\hat{\mathbf{r}} \cdot (\mathbf{u} + i\mathbf{v}) \exp(-i\omega t),\ r = \rho. \tag{7.1}$$

Here $\mathbf{u} + i\mathbf{v}$ is given by equation (5.6), with the $\mathbf{M}'$s being neglected, because they have no radial component, as is clear from equation (5.2). Apparently, $\hat{\mathbf{r}} \cdot (\mathbf{u} + i\mathbf{v})$ at $r = \rho$ is the radial component of the electric Mie field immediately beneath the surface of the metal sphere. On the other hand, $n_2^2 \hat{\mathbf{r}} \cdot (\mathbf{u} + i\mathbf{v})$ at $r = \rho$ is equal to the radial Mie field immediately outside the sphere, which is derived from the condition that the radial displacement current is continuous across the metal-air boundary. The difference between the above two radial electric fields leads to equation (7.1), which can be compared with equation (4.1).

At the third harmonic, the surface charge is

$$\sigma^{(3)} = \sum_{\ell=1}^{\infty} (2\ell + 1) \sum_m \frac{(\ell - m)!}{(\ell + m)!} b_{\ell m} P_\ell^m(\cos\theta) \cos m\phi \tag{7.2}$$

which is the expansion of $(\sigma + c.c.)^3$ in spherical harmonics, so that

$$b_{\ell m} = \frac{1}{4\pi} \int_0^{2\pi} d\phi \int_0^{\phi} (\sigma^3 + c.c.) P_\ell^m(\cos\theta) \cos m\phi \, d\theta \tag{7.3}$$

where again terms not proportional to $\exp(\pm i3\omega t)$ have been dropped, as they do not contribute to THG. It is easy to prove the selection rule that $b_{\ell m} = 0$ unless $m = 1$ or 3. Equations (7.2, 7.3) can be compared with equation (4.3). Dewitz *et al.* [9,10] replaced σ^3 in equation (7.3) with $\sigma\sigma^{(2)}$, where $\sigma^{(2)}$ is also found from equation (7.2), with σ^3 in equation (7.3) being replaced by σ^2. Therefore the integrand in equation (7.3) is always the product of three spherical harmonics, which can be evaluated analytically after lengthy algebra.

The electric field of THG scattering in air is

$$\sum_{\ell=1}^{\infty} \frac{2\ell + 1}{\ell(\ell + 1)} \sum_m \frac{(\ell - m)!}{(\ell + m)!} c_{\ell m} \mathbf{N}_{em\ell}^3(\mathbf{r}) \tag{7.4}$$

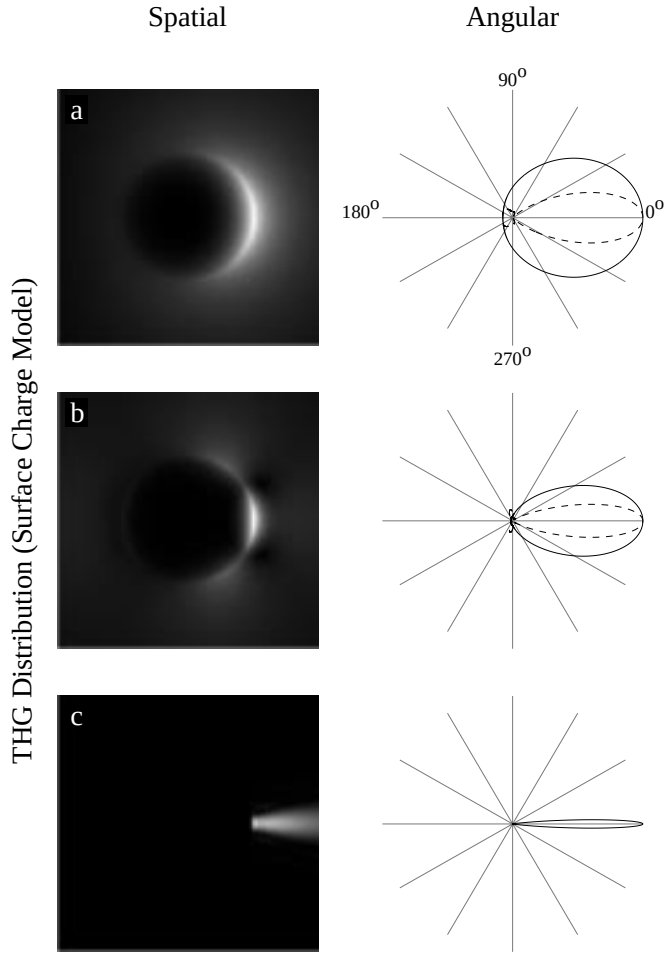

Fig. 7. Spatial and angular distributions of the electric field of THG scattering from the surface charge model. The conventions are the same as those in Figure 5.

where the $\mathbf{N}'$s are given by equation (5.2), with $3k_2^{(3)}$ in equations (5.2, 5.3) being replaced by $3k$, the wave number of THG light in air. Equation (7.4) can be compared with equation (5.12). Inside the metal sphere the electric field of the THG light is a series in $\mathbf{N}^1_{em\ell}(\mathbf{r})$ (see Eq. (5.2)). The tangential components of this internal THG field must equal those of equation (7.4). The radial component of this internal THG field is subtracted to that of equation (7.4), and the result must equal equation (7.2), giving

$$c_{\ell m} = \frac{-(3k\rho)^2\psi'_\ell(3n_2^{(3)}k\rho)}{n_2^{(3)}\psi_\ell(3n_2^{(3)}k\rho)\zeta_\ell^{(1)'}(3k\rho) - \psi'_\ell(3n_2^{(3)}k\rho)\zeta_\ell^{(1)}(3k\rho)} b_{\ell m}. \quad (7.5)$$

The fundamental law, that the tangential magnetic field of THG light must be continuous across the metal surface, cannot be satisfied. We use equation (7.4) and the Mie theory to find the magnetic field of THG scattering.

We use equations (7.4, 7.5) and the first line of equation (2.13) to find THG. In Figure 4c the cross-sections of both the total and backward THG scattering drop quickly to vanishingly small values, quite different from the cross-sections of Figure 4b. It is clear from Figure 7 that, while the surface charge model produces some backward THG scattering, the strength of this scattering is much weaker than that in Figure 6. This appears to arise from the polarization of the incident plane wave, whose electric field is in the x-direction, more or less tangential to the surface of the metal sphere (Fig. 3). However, the surface charge model ignores any electric field tangential to the metal surface, so that THG is greatly distorted. We may further appreciate the nature of this model through Huygens principle, according to which Mie scattering is produced by wavelets emitted from the surface of the metal sphere, whose electric fields are all in the radial direction, on account of metal conductivity. In the surface charge model the above surface Mie wavelets are taken to be the source of THG, with their amplitudes cubed and frequency shifted to the third harmonic, so that the pattern of THG scattering resembles that of Mie scattering. Indeed, Figure 7 resembles Figure 5 more closely than Figure 6.

8 Conclusions

We have used the Green function method to study THG scattering from metal surfaces. Our results are consistent with a previous study by Bloembergen *et al.* [12], who used a different method, when the metal surface is planar; but differ significantly from the results of the surface charge model [9,10], whether the metal surface is planar or spherical. In particular this model does not produce the strong backward scattering from the metal sphere, which is a particular non-linear phenomenon. In this case the surface charge model is not an adequate alternative to the Green function method, because THG takes place beneath the metal surface, where the radiation field is not dominated by the normal component. However, the long-established concept of surface charge can still be used successfully under other circumstances, as is mentioned in Section 4.

The authors thank Professor J. C. Earnshaw for helpful comments.

References

1. C.C. Wang, Phys. Rev. **178**, 1457 (1968).
2. C.K. Chen, A.R.B. de Castro, Y.R. Shen, Phys. Rev. Lett. **46**, 145 (1981).
3. G.T. Boyd, J.R.R. Leite, Y.R. Shen, Phys. Rev. B **30**, 519 (1984).
4. P.M. Morse, H. Feshbach, *Methods of Theoretical Physics* (International student edn., New York, McGraw-Hill, 1953).
5. F. Hache, D. Richard, C. Girad, Phys. Rev. B **38**, 7990 (1988).

6. G.S. Agarwal, S.D. Gupta, Phys. Rev. A **38**, 5678 (1988).
7. H. Chew, P.J. McNulty, M. Kerker, Phys. Rev. A **13**, 396 (1976).
8. S.C. Hill, D.H. Leach, R.K. Chang, J. Opt. Am. B **10**, 16 (1993).
9. J.P. Dewitz, W. Hübner, K.H. Bennemann, Z. Phys. D. **37**, 75 (1996).
10. D. Östling, P. Stampfli, K.H. Bennemann, Z. Phys D **28**, 169 (1993).
11. P.B. Johnson, R.W. Christy, Phys. Rev. B **9**, 5056 (1974).
12. N. Bloembergen, P.S. Pershan, Phys. Rev. **128**, 606 (1962).
13. M. Born, E. Wolf, *Principles of Optics*, 6th edn. (Oxford, Pergamon, 1989).
14. R.L. Sutherland, *Handbook of Nonlinear Optics* (New York, Basel, Hong Kong, Marcel Dekker, 1996).
15. M. Abramowitz, I.A. Stegun, *Handbook of Mathematical Functions*, 9th edn. (New York, Dover, 1972).
16. G. Mie, Ann. Phys. **25**, 377 (1908).